

Free convection from a heated vertical cylinder embedded in a fluid-saturated porous medium

A. P. Bassom, Sydney, Australia, and D. A. S. Rees, Bath, U.K.

(Received October 19, 1994; revised December 22, 1994)

Summary. We consider the free convection boundary layer flow induced by a heated vertical cylinder which is embedded in a fluid-saturated porous medium. The surface of the cylinder is maintained at a temperature whose value above the ambient temperature of the surrounding fluid varies as the n^{th} power of the distance from the leading edge. Asymptotic analyses and numerical calculations are presented for the governing nonsimilar boundary layer equations and it is shown that, when $n < 1$, the asymptotic flowfield far from the leading edge of the cylinder takes on a multiple-layer structure. However, for $n > 1$, only a simple single layer is present far downstream, but a multiple layer structure exists close to the cylinder leading edge. We have shown that the fully numerical and asymptotic calculations are in satisfactory agreement, especially for exponents n close to zero. Comparisons of the present numerical solutions obtained using the Keller-box method with previous numerical solutions using local methods are also given.

List of symbols

a	radius
f, \hat{f}, F, \hat{F}	scaled streamfunctions
f_0, f_1, f_2	inner zone streamfunctions when $n < 1$
F_{00}, \hat{F}_{00}	leading order streamfunctions in $n > 1$, $\xi \gg 1$ asymptotic solution
\bar{F}_0, \bar{F}_1	outer zone streamfunctions when $n < 1$
G	large parameter satisfying $G = X^2 \ln G$
g	gravitational acceleration
K	permeability of the porous medium
n	exponent in prescribed temperature law
r	radial co-ordinate
\bar{r}	rescaled radial co-ordinate
R	Darcy-Rayleigh number
T	temperature of convective fluid
T_w	temperature of cylinder at leading edge
T_∞	ambient temperature of fluid
u	velocity in axial direction
v	velocity in azimuthal direction
w	velocity in radial direction
x	axial co-ordinate
\bar{x}	rescaled axial co-ordinate
X	dimensionless axial co-ordinate
α	thermal diffusivity of the saturated medium
β	coefficient of thermal expansion
γ	constant in the boundary conditions for \bar{F}_0
ζ	dimensionless radial co-ordinate
$\bar{\zeta}$	co-ordinate for the outer zone in the $n < 1$ solution
$\eta, \hat{\eta}$	scaled radial co-ordinates

Θ	scaled fluid temperature
ϑ	similarity variable for the $n = 1$ problem
λ	nondimensionalisation constant (Eq. (9))
μ	viscosity of fluid
$\xi, \hat{\xi}$	scaled axial co-ordinates
ρ	density of fluid
τ	co-ordinate for the inner zone in the $n < 1$ solution
ϕ	azimuthal co-ordinate
$\varphi, \hat{\varphi}$	similarity variables for the $n > 1$ problem
ψ	streamfunction

1 Introduction

In this paper we consider the free convective boundary layer flow induced by a heated vertical cylinder embedded in a fluid-saturated porous medium. The surface temperature of the cylinder is taken to be proportional to x^n , where x is the dimensional distance from the leading edge/base of the cylinder. The Darcy-Rayleigh number, R , is assumed to be large, thereby allowing a boundary layer analysis to be undertaken.

Minkowycz and Cheng [1] were the first authors to study this problem. In their paper numerical results for various values of n lying between 0 and 1 were presented and comparisons between the local similarity and local nonsimilarity methods of solution were given. Their detailed temperature profiles show that the boundary layer thickens dramatically as x increases. Merkin [2], on the other hand, confined himself to the constant temperature case, $n = 0$. He presented (i) a numerical solution of the governing nonsimilar boundary layer equations using a nonlocal marching method coupled to a parabolic solver, and (ii) an asymptotic analysis for large values of x . He found that the boundary layer evolves into a two-layer structure at large distances from the leading edge. In this paper we extend the work of [2] by considering a range of values of the power-law exponent, n . The governing equations are also solved numerically using the Keller-box scheme in order to assess the accuracy of the 'local' methods used in [1], and to compare with the present asymptotic results.

Other papers which study variations of the present problem include that of Merkin and Pop [3], which analyses mixed convection from a uniformly heated cylinder, Kumari and Nath [4] which investigates non-Darcy mixed convection from a uniformly heated cylinder, and Hossain and Nakayama [5] which considers non-Darcy free convection from a constant heat flux cylinder. Both [4] and [5] contain only numerical results for their respective problems.

2 Formulation of the problem

We consider the cylindrical polar coordinate system, (x, ϕ, r) corresponding to the axial, azimuthal and radial directions, respectively, and denote the associated fluid velocities as (u, v, w) ; the configuration is shown in Fig. 1. Assuming axisymmetry, for which $v = 0$ and all other dependent variables are independent of ϕ , the continuity equation takes the form

$$\frac{\partial}{\partial x}(ru) + \frac{\partial}{\partial r}(rw) = 0. \quad (1)$$

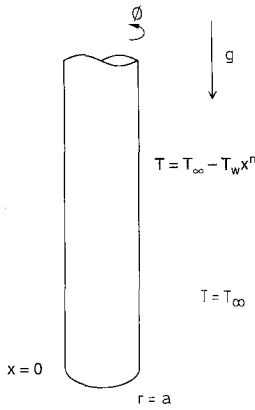


Fig. 1. Definition sketch of the flow domain and coordinate system

Furthermore, Darcy's law subject to the boundary layer and Boussinesq approximations may be written as

$$u = \frac{K}{\mu} \rho g \beta (T - T_{\infty}), \quad (2)$$

where T_{∞} is the ambient temperature of the fluid, K is the permeability of the medium, g is the gravitational acceleration, β is the coefficient of thermal expansion, and ρ and μ are the density and viscosity of the fluid, respectively. The specification of the problem is completed by the energy equation, which can be expressed in the form

$$u \frac{\partial T}{\partial x} + w \frac{\partial T}{\partial r} = \alpha \left(\frac{\partial^2 T}{\partial r^2} + \frac{1}{r} \frac{\partial T}{\partial r} \right) \quad (3)$$

where the boundary layer approximation has again been invoked and α denotes the thermal diffusivity of the saturated medium. In (3) the first derivative term on the right hand side has been retained since we shall be considering those cases for which r is of the same order of magnitude as the cylinder radius. The boundary conditions for a power-law surface temperature distribution are

$$w = 0, \quad T = T_{\infty} + T_w x^n \quad \text{on } r = a, \quad (4.1)$$

and

$$u \rightarrow 0, \quad T \rightarrow T_{\infty} \quad \text{as } r \rightarrow \infty, \quad (4.2)$$

where a is the radius of the cylinder. Thus the cylinder is assumed to be impermeable, and there is no disturbance to the far-field, at least to leading order. We non-dimensionalise this problem using the scalings given by Merkin [2], and it is convenient to define a streamfunction ψ according to

$$u = \frac{1}{r} \frac{\partial \psi}{\partial r} \quad w = -\frac{1}{r} \frac{\partial \psi}{\partial x}. \quad (5.1, 2)$$

The co-ordinates are rescaled by

$$x = aR\bar{x}, \quad r = a\bar{r}, \quad (5.3, 4)$$

where the Darcy-Rayleigh number R is defined to be $R = K g \rho \beta a T_w / (8^n \mu \alpha)$. The transformations

$$\psi = \frac{1}{2} \alpha a R \hat{\xi} \hat{f}(\hat{\xi}, \hat{\eta}), \quad T - T_\infty = \frac{T_w}{8^n} \Theta(\hat{\xi}, \hat{\eta}), \quad \hat{\eta} = \hat{\xi}^{-1}(\bar{r}^2 - 1), \quad \hat{\xi} = 2(\sqrt{2\bar{x}}), \quad (6)$$

reduce Eq. (2) to the relationship $\Theta = \hat{f}_{\hat{\eta}}$, and the energy equation (3) becomes

$$(1 + \hat{\xi} \hat{\eta}) \hat{f}_{\hat{\eta}\hat{\eta}} + (\hat{\xi} + \hat{f}) \hat{f}_{\hat{\eta}} = \hat{\xi}(\hat{f}_{\hat{\xi}\hat{\eta}} \hat{f}_{\hat{\eta}} - \hat{f}_{\hat{\eta}\hat{\xi}} \hat{f}_{\hat{\xi}}), \quad (7)$$

which is to be solved subject to the requirements that

$$\hat{f}(0) = 0, \quad \hat{f}'(0) = \hat{\xi}^{2n} \quad \text{on} \quad \hat{\eta} = 0; \quad \hat{f}' \rightarrow 0 \quad \text{as} \quad \hat{\eta} \rightarrow \infty. \quad (8)$$

When $n = 0$ this system is identical to that obtained in [2], and we now rescale by writing

$$\hat{\xi} = \lambda \xi, \quad \hat{\eta} = \lambda^{-1} \eta \quad \text{and} \quad \hat{f} = \lambda^{2n-1} f, \quad (9)$$

where $\lambda^{2(1-n)} = 2$. This is possible whenever $n \neq 1$, and then we are left with

$$(1 + \xi \eta) f_{\eta\eta} + \left(\xi + \frac{1}{2} f \right) f_{\eta} = \frac{1}{2} \xi (f_{\xi\eta} f_{\eta} - f_{\eta\xi} f_{\xi}), \quad (10.1)$$

subject to the conditions that

$$f(0) = 0, \quad f_{\eta}(0) = \xi^{2n} \quad \text{on} \quad \eta = 0; \quad f_{\eta} \rightarrow 0 \quad \text{as} \quad \eta \rightarrow \infty. \quad (10.2-4)$$

The principal reason for making this transformation is that, when $n = 0$, the solution near the leading edge is identical to leading order to the similarity solution for a vertical flat plate given by Cheng and Minkowycz [6].

In view of the boundary condition (10.3) on f_{η} , it is clear that the solution of Eq. (10) at the origin would seem to be precisely zero when $n > 0$. This indicates that the definition of the pseudo-similarity variable, η , has the wrong form near the leading edge. It is necessary, then, to introduce one more re-definition of co-ordinates in order to avoid this difficulty. We therefore define

$$\zeta = \eta \xi^n, \quad X = \xi^{1-n}, \quad f = X^{n/(1-n)} F(X, \zeta), \quad (11)$$

in Eq. (10) to obtain the system

$$(1 + X\zeta) F_{\zeta\zeta} + \left(X + \frac{1}{2} F \right) F_{\zeta} = \frac{1}{2} (1 - n) X (F_{\zeta} F_{X\zeta} - F_X F_{\zeta\zeta}) + \frac{1}{2} n (2F_{\zeta}^2 - F F_{\zeta\zeta}) \quad (12.1)$$

$$F(0) = 0, \quad F_{\zeta}(0) = 1 \quad \text{on} \quad \zeta = 0, \quad (12.2, 3)$$

$$F_{\zeta} \rightarrow 0 \quad \text{as} \quad \zeta \rightarrow \infty. \quad (12.4)$$

This latest form is the one most suitable for numerical computation for two main reasons. First, the solution for F at the origin is now clearly non-zero. Secondly, the subsequent development of the flow profile is expressible in terms of a power series in X which is composed of integer powers for all values of n , rather than fractional powers. Furthermore, Eqs. (12) are exactly equivalent to Eqs. (21)–(24) of Minkowycz and Cheng [1].

3 Asymptotic solution far downstream from the leading edge

We now consider the structure of the boundary layer at large distances along the axis of the cylinder. It is found that the form of the solution of (7) and (8) for $\hat{\xi} \gg 1$ is critically dependent on the value of the power law exponent n . It was pointed out by Minkowycz and Cheng [1] that when $n = 1$ then this system admits an exact similarity solution, for if $\vartheta = \hat{\xi}\hat{\eta}$ and $\hat{f} = \hat{\xi}\hat{F}(\vartheta)$ then

$$(1 + \vartheta) \hat{F}''' + (1 + 2\hat{F}) \hat{F}'' = 2(\hat{F}')^2; \quad \hat{F}(0) = 0, \quad \hat{F}'(0) = 1, \quad \hat{F}'(\infty) = 0.$$

To explain the structure of the boundary layer for large $\hat{\xi}$ when $n \neq 1$ it is convenient to revert to system (10). When $n > 1$, we define a new variable $\varphi = \eta\xi^n$; therefore for $\varphi = O(1)$ we are considering a zone which is asymptotically thinner than that for the $n = 1$ case discussed immediately above. We seek a solution of (10) which commences

$$F = \xi^n [F_{00}(\varphi) + \dots], \tag{13.1}$$

and it is a routine task to verify that

$$F_{00}''' + \frac{1}{2} (1 + n) F_{00} F_{00}'' - n(F_{00}')^2 = 0;$$

$$F_{00}(0) = 0, \quad F_{00}'(0) = 1, \tag{13.2}$$

$$F_{00}' \rightarrow 0 \quad \text{as} \quad \varphi \rightarrow \infty.$$

A numerical solution of this equation is given in Fig. 2 for various values of n . We should point out that, for large values of n , it is possible to identify the asymptotic structure which is taken on by F_{00} . In this limit it turns out that $F_{00} = O(1/\sqrt{n})$, and the region over which it adjusts itself to the requisite final asymptotic form shrinks to become $\varphi = O(1/\sqrt{n})$. If we here define $\varphi = \hat{\phi}/\sqrt{n}$ and $F_{00}(\varphi) = \hat{F}_{00}(\hat{\phi})/\sqrt{n} + \dots$ then problem (13.2) becomes, at leading

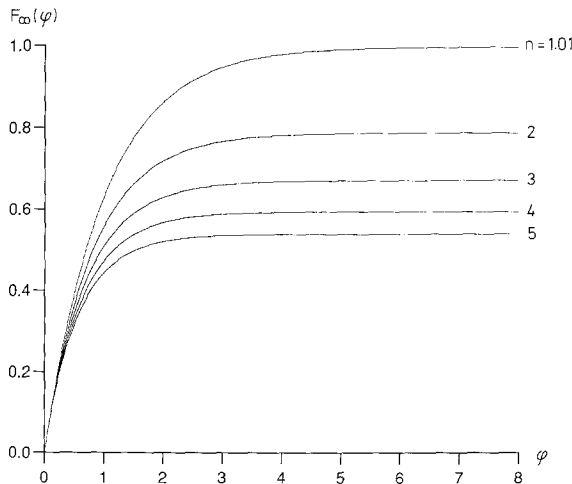


Fig. 2. Solutions of Eq. (13.2) for $F_{00}(\varphi)$ corresponding to the far-downstream boundary layer profile when $n > 1$. Shown are the cases $n = 1.01, 2, 3, 4$ and 5

order,

$$\begin{aligned}\hat{F}_{00}''' + \frac{1}{2} \hat{F}_{00} \hat{F}_{00}'' - (\hat{F}_{00}')^2 &= 0; \\ \hat{F}_{00}(0) &= 0, \quad \hat{F}_{00}'(0) = 1, \\ \hat{F}_{00}' &\rightarrow 0 \quad \text{as } \hat{\phi} \rightarrow \infty,\end{aligned}\tag{13.3}$$

where dashes in Eq. (13.3) represent differentiation with respect to $\hat{\phi}$. We can conclude from Eqs. (13) and Fig. 2 that, whenever $n > 1$, the flow structure for $\xi \gg 1$ is relatively simple, for the flow is confined to a single region of asymptotic thickness $O(\xi^{-n})$ immediately adjacent to the cylinder surface. However, this simplicity does not carry across into the $n < 1$ case for which, remembering that $\xi \gg 1$, it is found (after some experimentation) that it is convenient to define the large parameter G according to

$$G = \xi^{2(1-n)} \ln G.\tag{14}$$

It is then easily shown, using an extension of the argument presented in [2], that we would expect the flowfield to take a two-layered form. The outer zone has depth $O(G^{-1}\xi)$; here we define the scaled variable $\bar{\zeta} = \xi\eta/G$ and look for a solution of (10) which takes the form

$$f = \xi[\bar{F}_0(\bar{\zeta}) + (\ln G)^{-1} \bar{F}_1(\bar{\zeta}) + \dots].\tag{15}$$

An analysis of (10) then shows that \bar{F}_0 and \bar{F}_1 satisfy the equations

$$\bar{\zeta} \bar{F}_0''' + (1 + \bar{F}_0) \bar{F}_0'' = n(\bar{F}_0')^2,\tag{16.1}$$

$$\bar{\zeta} \bar{F}_1''' + (1 + \bar{F}_0) \bar{F}_1'' - 2n\bar{F}_0' \bar{F}_1' + \bar{F}_0'' \bar{F}_1 = (n-1)(\bar{F}_0')^2.\tag{16.2}$$

In order to satisfy the far-field conditions as $\eta \rightarrow \infty$ we require that $\bar{F}_0', \bar{F}_1' \rightarrow 0$ as $\bar{\zeta} \rightarrow \infty$, but it is straightforward to verify that the derivative boundary condition (10.3) on the cylinder surface cannot be satisfied using these functions. Therefore some kind of inner structure is suggested and, in order to examine this, it is necessary to consider the behaviour of \bar{F}_0 and \bar{F}_1 as $\bar{\zeta} \rightarrow 0$. It may be shown that in this limit these functions develop series solutions of the form

$$\sum_i \sum_j a_{ij} \bar{\zeta}^i (-\ln \bar{\zeta})^j,\tag{17}$$

where $a_{ij} = 0$ when $i < j$. It is a routine task to obtain recurrence relations which link these constants but, for the purpose of matching between \bar{F}_0, \bar{F}_1 and the inner solution, it is sufficient to note that

$$\bar{F}_0 \rightarrow -\bar{\zeta} \ln \bar{\zeta} + \gamma \bar{\zeta} + \frac{1}{2} n \bar{\zeta}^2 (\ln \bar{\zeta})^2 + \dots, \quad \text{and}\tag{18.1}$$

$$\bar{F}_1 \rightarrow K \bar{\zeta} \ln \bar{\zeta} + \dots\tag{18.2}$$

as $\bar{\zeta} \rightarrow 0$, where γ has to be determined numerically and K is specified below. In Fig. 3 we show the form of $\bar{F}_0(\bar{\zeta})$ for various values of n ; these curves were computed using a modified form of the Keller box method which uses the series solution (17) at $\bar{\zeta} = 0.2$ to provide initial conditions in terms of γ , which is computed as part of the solution procedure.

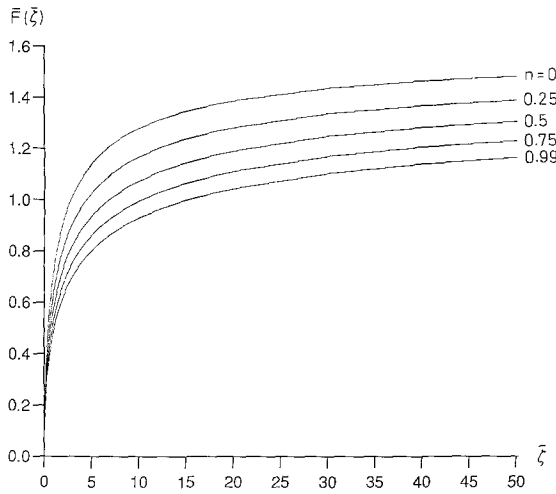


Fig. 3. Solutions of Eq. (16.1) for $\bar{F}_0(\bar{\xi})$ corresponding to the far-downstream outer-layer boundary layer profile when $n < 1$. Shown are the cases $n = 0, 0.25, 0.5, 0.75$ and 0.99

Now in order to satisfy boundary condition (10.3), we need to examine an inner layer of depth $O(\xi^{-1})$, which is the appropriate scaling on which the necessary viscous balance holds. If we now define $\tau = \xi\eta = O(1)$, then the limiting forms (18.1, 2) suggest that

$$f = \xi^{2n-1}[f_0(\tau) + (\ln G)^{-1}f_1(\tau) + (\ln G)^{-2}f_2(\tau) + \dots]. \tag{19}$$

Substitution of (19) in (10.1), imposition of (10.2, 3), and suitable matching with the outer solutions \bar{F}_0 and \bar{F}_1 yield

$$f_0 = \tau, \quad f_1 = \tau - (1 + \tau) \ln(1 + \tau), \quad f_2 = (1 - \gamma)f_1, \tag{20}$$

and the matching process forces us to the conclusion that the constant K in (18.2) is related to γ by the simple relation $\gamma - 1 = K$. In the next Section we shall consider the heat flux coefficient for the boundary layer, and, in terms of the variables in (10), this coefficient is proportional to $d^2f/d\eta^2|_{\eta=0}$. Consequently, for $\xi \gg 1$ this function takes the form

$$\frac{d^2f}{d\eta^2}\Big|_{\eta=0} = \xi^2 \frac{d^2f}{d\tau^2}\Big|_{\tau=0} = \frac{\xi^2}{\ln G} \left[-1 + \frac{(\gamma - 1)}{\ln G} + \dots \right]. \tag{21}$$

We shall examine the comparison between this prediction and the corresponding, numerically determined, heat flux in Section 4. However, we could expect to improve the accuracy of the comparison by taking further terms in expansion (19) which proceeds, a least initially, in inverse powers of $\ln G$. In order to compute the necessary constants which arise it would be necessary to numerically solve higher order equations for the outer layer ($\bar{\xi} = O(1)$) flow of which (16.2) is the next in the hierarchy. This particular equation was solved by Merkin [2] for the constant cylinder temperature case, $n = 0$, but in this work we shall not examine these further orders for general values of n .

It should be remarked that, when $n > 1$, the asymptotic form of the solution of (10) for $\xi \ll 1$ is very similar to that for the far-downstream behaviour of the flow when $n < 1$, as described immediately above. For $n > 1$ and $\xi \ll 1$, the boundary layer again divides into two distinct sublayers; the inner region is of depth $O(\xi^{-1})$ and the outer is of extent $O(\xi^{-1}G)$, where G is as defined in (14). In the inner zone it is easy to show that $F = O(\xi^{n-1})$ and thus is small. Given this outline, it follows that the details of the structure are completely analogous to those presented in

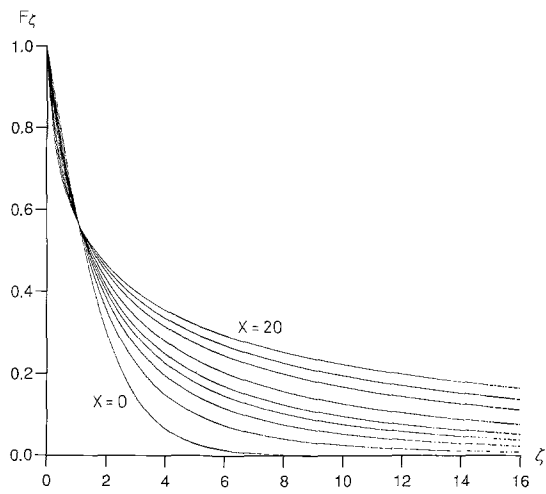
(13)–(21), so they will not be presented for the sake of brevity; however the most important point is that as $\xi \rightarrow 0$ the thickness of the boundary layer appears to grow without limit. This fact, together with the two-layer asymptotic structure, represents an insurmountable barrier for solving numerically the equations as posed here. The simplest way to avoid such a numerical difficulty lies in modifying the problem to one where the heated cylinder has a temperature at the leading edge which is above the ambient temperature of the medium, and where the surface temperature profile has a power law variation relative to the leading-edge value. In this case the leading edge problem is well-posed, numerically, and the large distance asymptotic structure remains intact.

4 Numerical solution

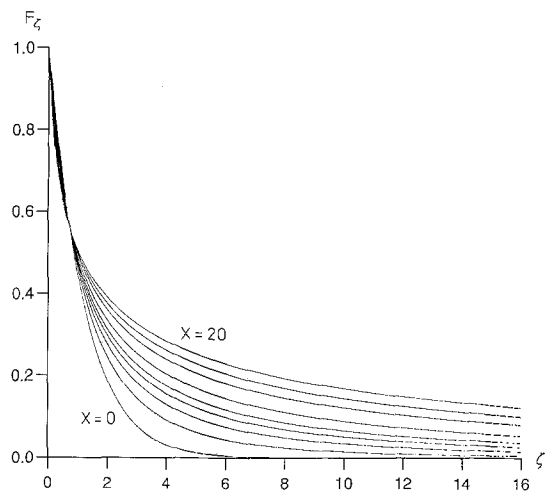
In this Section we present a selection of numerical solutions of Eqs. (12). We shall restrict attention to those cases for which $0 \leq n < 1$ since when $n = 1$ the transformation (9) is invalid and the flow is self-similar, as was shown in [1]. Furthermore, for larger values of n , the boundary layer develops a two-zoned asymptotic structure as $\xi \rightarrow 0$ which becomes infinitely wide as $\xi \rightarrow 0$ so it is clearly impossible to begin a numerical computation of the flow near there. However, the analysis of the last Section has demonstrated the precise form of the asymptotic structure far from the leading edge of the cylinder whenever $n > 1$ (see (13)). Finally we note that when $n < 0$ the temperature becomes infinite at the leading edge, an effect which clearly cannot be realised in practice, although it is quite possible to obtain numerical solutions for negative values of n which are not too large in magnitude. Thus we concentrate on those cases for which $0 \leq n < 1$.

We have used the Keller-box scheme to solve system (12); the particular version used a numerically computed Jacobian in the Newton-Raphson part of the algorithm, rather than one which is defined explicitly within the code. Thus only the right hand side of the matrix/vector iteration scheme is entered into the code, thereby reducing both the code development time and the risk of programming errors. Convergence of the Newton-Raphson algorithm was deemed to have taken place when the maximum absolute change between successive iterates was less than 10^{-8} . Double precision arithmetic was used throughout. In the X -direction a uniform grid of constant step 0.05 was chosen, and integrations up to $X = 20$ were performed. A nonuniform basic grid of 116 points in the ζ -direction was specified in which ζ varied between 0 and 10^6 ; such a large value of ζ_{\max} was necessary because the boundary layer thickness increases dramatically whilst marching downstream. Checks were made that $\zeta_{\max} = 10^6$ is sufficiently large by repeating the calculations with $\zeta_{\max} = 10^3, 10^4$, and 10^5 . Typically, it was found that values of $F_{\zeta\zeta}(X = 20, \zeta = 0)$ vary in only the sixth significant figure when changing ζ_{\max} from 10^5 to 10^6 . Highly accurate solutions were then obtained by solving the equations on successively finer grids and using Richardson Extrapolation.

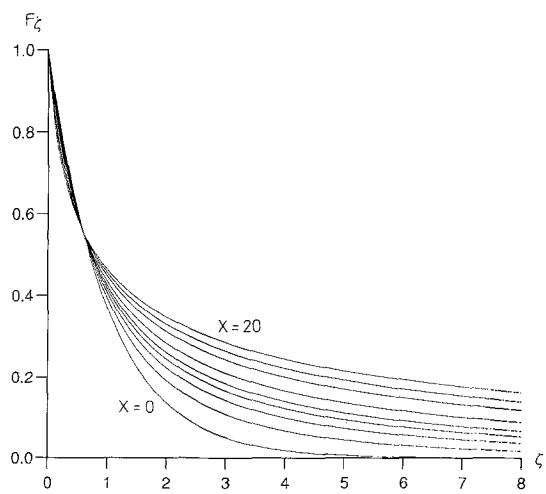
In Fig. 4a–c we display the developing profiles of F_ζ as X increases; the respective power-law exponents $n = 0, n = 0.5$ and $n = 0.99$ are shown. Following from definitions (6), the function F_ζ is both a scaled temperature and a scaled vertical velocity. All three subfigures comprising Fig. 4 illustrate that the boundary layer thickness grows very quickly as the distance from the leading edge increases. Further, the slope of the profiles at $\zeta = 0$, which is proportional to the local rate of heat transfer, becomes increasingly negative as X increases. These qualitative features of the developing profiles are also true for other values of n whenever $n < 1$. Thus the numerical results confirm the asymptotic prediction of a two-layer structure.



a



b



c

Fig. 4. Profiles of F_ζ , the scaled temperature, as a function of ζ at the following values of X : $X = 0, 0.5, 1.0, 1.5, 2, 3, 5, 10, 20$. **a** $n = 0$, **b** $n = 0.5$, **c** $n = 0.99$

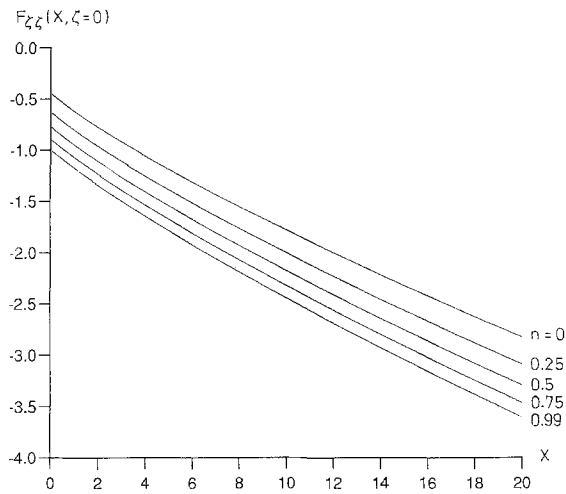


Fig. 5. Variation with X of the computed local rate of heat transfer, $F_{\zeta\zeta}(X, \zeta = 0)$, for the following values of n : $n = 0, 0.25, 0.5, 0.75$ and 0.99

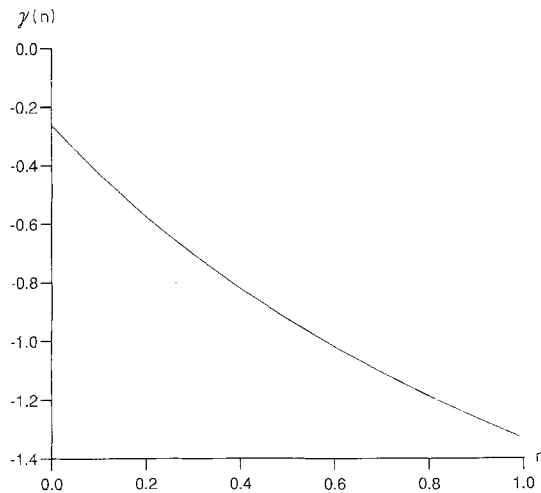


Fig. 6. Variation of γ with n

Figure 5 shows the variation of $F_{\zeta\zeta}(X, 0)$, the scaled local heat flux at the surface of the cylinder, for various values of n . The increasing slopes of the temperature profiles shown in Fig. 4 are reflected in the behaviours shown in Fig. 5. Detailed comparisons of some of these values with those obtained by Minkowycz and Cheng [1], who used a local similarity method and a local non-similarity method, are shown in the following tables. In these, LS and NLS refer respectively to the local similarity and local nonsimilarity solutions given in [1], and KB to the present Keller-box computations. The results indicate that, while the local methods of [1] give quite accurate results for the scaled rate of heat transfer for small values of X when compared with the present Keller-box computations, they begin to diverge as X increases above about 6. As the maximum value of ζ used by Minkowycz and Cheng [1] (termed η in their paper) is not quoted, we do not know at this stage whether the divergence is caused by the inadequacy of local methods or by an insufficiently large ζ_{\max} in their results.

If we recall definition (14) for the large parameter G and transformations (11) for the variables,

it is an elementary task to verify that the asymptotic result (21) for the heat flux translates to

$$F_{\zeta\zeta}(X, 0) = \frac{X}{\ln G} \left(-1 + \frac{(\gamma - 1)}{\ln G} + \dots \right), \quad (22)$$

where $\gamma = \gamma(n)$ is defined by having the solution of (16.1) satisfy the boundary condition (18.1). The variation of γ with n is shown in Fig. 6. In Table 4 we give a comparison between (22) and the numerically determined values for $F_{\zeta\zeta}(X, 0)$ at $X = 0$. As the series solution, (22), proceeds as an inverse logarithmic series, it is not to be expected that close quantitative agreement between the asymptotic and numerical solutions should be found at a value of X as low as 20. However, it is clear from Table 4 that we have surprisingly close results. When $n = 0$ the agreement is excellent; the numerical and asymptotic results agree to within 1.2 percent, but this agreement worsens with increasing n .

Table 1. Values of $-F_{\zeta\zeta}(X, \zeta = 0)$ for $n = 0$

X	LS	LNS	KB
0.00	0.4438	0.4438	0.4438
0.25	0.4855	0.4899	0.4901
0.50	0.5272	0.5332	0.5347
0.75	0.5664	0.5747	0.5776
1.00	0.6049	0.6149	0.6191
2.00	0.7517	0.7668	0.7750
3.00	0.8915	0.9085	0.9191
4.00	1.024	1.044	1.055
5.00	1.154	1.176	1.185
6.00	1.283	1.305	1.310
7.00	1.413	1.435	1.431
8.00	1.544	1.565	1.549
9.00	1.678	1.696	1.665
10.00	1.815	1.830	1.777

Table 2. Values of $-F_{\zeta\zeta}(X, \zeta = 0)$ for $n = 0.25$

X	LS	LNS	KB
0.00	0.6266	0.6266	0.6266
0.25	0.6748	0.6729	0.6726
0.50	0.7186	0.7175	0.7172
0.75	0.7609	0.7604	0.7604
1.00	0.8021	0.8023	0.8025
2.00	0.9587	0.9607	0.9616
3.00	1.106	1.110	1.110
4.00	1.268	1.252	1.250
5.00	1.381	1.391	1.385
6.00	1.518	1.529	1.514
7.00	1.655	1.667	1.640
8.00	1.795	1.806	1.763
9.00	1.937	1.947	1.882
10.00	2.083	2.091	1.999

Table 3. Values of $-F_{\zeta\zeta}(X, \zeta = 0)$ for $n = 0.5$

X	LS	LNS	KB
0.00	0.7704	0.7704	0.7704
0.25	0.8177	0.8167	0.8162
0.50	0.8620	0.8616	0.8610
0.75	0.9050	0.9052	0.9045
1.00	0.9471	0.9478	0.9470
2.00	1.106	1.110	1.109
3.00	1.259	1.263	1.260
4.00	1.405	1.409	1.404
5.00	1.549	1.553	1.541
6.00	1.691	1.696	1.674
7.00	1.835	1.839	1.804
8.00	1.980	1.984	1.930
9.00	2.127	2.130	2.052
10.00	2.278	2.280	2.173

Table 4. Comparison of numerically and asymptotically determined predictions of $F_{\zeta\zeta}(X = 20, \zeta = 0)$ for various values of n

n	γ	Asymptotic	Numerical	% Difference
0.00	-0.26168	-2.8614	-2.8249	1.2
0.25	-0.64242	-2.9780	-3.0889	3.7
0.5	-0.92475	-3.0644	-3.2939	7.4
0.75	-1.14772	-3.1327	-3.4644	10.6
0.99	-1.32463	-3.1869	-3.6065	13.2

5 Closing remarks

In this paper we have presented a combined asymptotic and numerical analysis of the flow and heat transfer induced by a vertical cylinder which has a surface temperature given by a power-law distribution. Asymptotic results have been found relating to the whole of the power-law exponent range which makes physical sense and it thereby extends the constant surface temperature analysis of Merkin [2]. Various asymptotic properties of the flow have been detailed, and we have shown that the quantitative agreement between asymptotic predictions and numerical computations is generally satisfactory, and is especially good for small values of the exponent n . Apart from the $n = 1$ case, for which the flow is self-similar, the resulting nonsimilar flow always has a two-layer structure merging into a single layer structure, or vice versa. When $n < 1$, the two-layer structure appears as $\xi \rightarrow \infty$, whereas when $n > 1$, it appears as $\xi \rightarrow 0^+$.

Attention has been given to producing an accurate set of numerical results, and we have therefore improved on the earlier study of Minkowycz and Cheng [1] in two ways. Firstly, we have made use of a nonlocal marching method (the Keller-box scheme) to solve the parabolic governing equations, and, secondly, we have taken great care to ensure that the outer edge of the evolving boundary layer is contained well within the computational domain. We have confirmed that techniques based on local similarity and local nonsimilarity methods, used in [1], are quite adequate for small distances downstream of the leading edge of the cylinder; however these methods are of decreasing accuracy as the streamwise co-ordinate increases.

References

- [1] Minkowycz, W. J., Cheng, P.: Free convection about a vertical cylinder embedded in a porous medium. *Int. J. Heat. Mass Transfer* **19**, 805–813 (1976).
- [2] Merkin, J. H.: Free convection from a vertical cylinder embedded in a porous medium. *Acta Mech.* **62**, 19–28 (1986).
- [3] Merkin, J. H., Pop, I.: Mixed convection boundary-layer on a vertical cylinder embedded in a porous medium. *Acta Mech.* **66**, 251–262 (1987).
- [4] Kumari, M., Nath, G.: Non-Darcy mixed convection boundary layer flow on a vertical cylinder in a saturated porous medium. *Int. J. Heat Mass Transfer* **32**, 183–187 (1989).
- [5] Hossain, M. A., Nakayama, A.: Non-Darcy free convective flow along a vertical cylinder embedded in a porous medium with surface mass flux. *Int. J. Heat. Fluid Flow* **14**, 385–390 (1993).
- [6] Cheng, P., Minkowycz, W. J.: Free convection about a vertical flat plate imbedded in a porous medium with application to heat transfer from a dike. *J. Geophys. Res.* **82**, 2040–2044 (1977).

Authors' addresses: A. P. Bassom, School of Mathematics, University of New South Wales, Sydney 2052, Australia (Permanent address: Department of Mathematics, University of Exeter, North Park Road, Exeter, Devon. EX44QE, U.K.), and D. A. S. Rees, School of Mech. Engineering, University of Bath, Claverton Down, Bath, BA27AY, U.K.